Oxidative conditions can lead to exceptional preservation through phosphatization

Pierre Gueriau, Sylvain Bernard, François Farges, Cristian Mocuta, Didier B Dutheil, Thierry Adatte, Brahimsamba Bomou, Marie Godet, Dominique Thiaudière, Sylvain Charbonnier, et al.

Oxidative conditions can lead to exceptional preservation through phosphatization

Pierre Gueriau[1,2,3], Sylvain Bernard[4], François Farges[4], Cristian Mocuta[1], Didier B. Dutheil[5], Thierry Adatte[3], Brahimsamba Bomou[3], Marie Godet[2], Dominique Thiaudière[1], Sylvain Charbonnier[5], and Loïc Bertrand[1,2]

[1]Synchrotron SOLEIL, l'Orme des Merisiers, BP 48 St Aubin, 91192 Gif-sur-Yvette, France

[2]Université Paris-Saclay, CNRS, ministère de la Culture, UVSQ, MNHN, Institut photonique d'analyse non-destructive européen des matériaux anciens, 91192, Saint-Aubin, France

[3]Institute of Earth Sciences, University of Lausanne, Géopolis, CH-1015 Lausanne, Switzerland

[4]Muséum National d'Histoire Naturelle, Sorbonne Université, CNRS, UMR 7590, Institut de Minéralogie, Physique des Matériaux et Cosmochimie, Paris, France

[5]Muséum national d'Histoire naturelle, Sorbonne Université, CNRS UMR 7207, CR2P, Centre de Recherche en Paléontologie - Paris, 8 rue Buffon, 75005, Paris, France

ABSTRACT

Exceptional preservation through phosphatization is primarily controlled by a reduction in pH, favoring the precipitation of apatite over that of calcite. Laboratory experiments suggested that phosphatization results from anoxic decay. Here we report results of the fine scale mineralogical characterization of Cretaceous phosphatized fossils of teleost fishes and crustaceans from the Jebel oum Tkout Lagerstätte (Morocco). Data collected using complementary laboratory and synchrotron-based X-ray techniques reveal that oxidative conditions were established at a certain step of decay. Supporting these conclusions are the presence, covering and embedded in the phosphatized tissues, of Fe(III)-rich mineral phases which precipitation was likely biologically-induced during decay. In contrast to the general belief, the present study highlights that the establishment of oxidative conditions during decay can be compatible with exceptional preservation of fossils through phosphatization.

INTRODUCTION

Soft tissue phosphatization, *i.e.*, calcium phosphate mineralization occurring prior to the degradational collapse of cellular tissues, provides the most spectacular fossils of animals, still exhibiting sub-cellular details (Martill, 1990; Briggs, 2003). Most of the time, soft tissues are pseudomorphically replaced by francolite (a carbonate-rich fluorapatite), as is the case of the ~110-Ma fossil fishes from the Santana Formation (Brazil) (Martill, 1988). Closed systems, such as those built by biofilms growing around carcasses, promote apatite precipitation by trapping phosphorus (Williams and Reimers, 1983; Martill, 1988; Briggs and Kear, 1993; Wilby et al., 1996**).** Laboratory experiments suggested that phosphatization results from a decay-induced fall

in pH under anaerobic conditions, the decrease of pH being responsible for a switch from carbonate to phosphate precipitation (Allison, 1988; Briggs and Kear, 1993; Briggs and Wilby, 1996; Sagemann et al., 1999). However, authigenic phosphates such as francolite may precipitate under a number of redox conditions, including oxic to suboxic conditions (Föllmi, 1996 and references therein). Phosphatization requires a sufficient concentration of phosphorous (Martill, 1988; Briggs and Kear, 1993; Briggs, 2003), and oxic conditions are known to enhance the release of phosphorus (e.g., Meunier-Christmann et al., 1989). Here, we report an in-depth and *in situ* assessment of the redox conditions having prevailed during the phosphatization of "exceptionally preserved" Cretaceous fossils of fishes and crustaceans from the Jebel oum Tkout (OT1) Lagerstätte of Morocco.

METHODS

A combination of advanced characterization tools, including X-ray diffraction (XRD), scanning electron microscopy (SEM) and infrared (IR) spectroscopy was used to achieve a micro-geochemical characterization of a series of fossils. In addition, major-to-trace elemental composition was determined using synchrotron-based micro X-ray fluorescence (μXRF) mapping at a spatial resolution of 60–100 μm and at detection limits of a few tens of ppm (Gueriau et al., 2014, 2018). Samples were scanned in air using a 17.2 keV beam allowing detection of elements from chlorine to uranium. At this energy, X-rays penetrate up to a couple of millimeters, but only the XRF photons from the first hundreds of microns can be collected (see Gueriau et al., 2018). The deconvolution of μXRF data allowed estimating the concentrations of all detected elements, including rare earth elements (REEs) that were then normalized to the Post-Archean Australian Shale (PAAS) reference (McLennan, 1989) to

reconstruct REE patterns, ratios and anomalies in the fossils at “local”, submillimeter scales (Gueriau et al., 2015). Finally, the redox states of Fe and Ce were determined using synchrotron-based micro-X-ray absorption spectroscopy (μXAS) at a 3–10 μm spatial resolution. For Fe, continuous Cauchy wavelet transformation of the spectra was performed to establish a more robust determination of the speciation (Munoz et al., 2003). Additional details on Methods are provided in the GSA Data Repository[1].

GEOLOGICAL AND PALEOENVIRONMENTAL CONTEXT

The Upper Cretaceous (Cenomanian, ~95 Myr) OT1 Lagerstätte from south-eastern Morocco (Fig. 1A) yielded a rich and well-preserved soft-bodied fauna including mollusks, insects, crustaceans, elasmobranchs and actinopterygian fishes embedded in a pale beige laminated mudstone carved by mudcracks (Fig. 1B), Absence of marine organisms and the presence of mudcracks, unionids and larvae of insects restricted to freshwater environments, strongly suggest a low-energy seasonally dried freshwater deposition environment (Dutheil, 1999; Garassino et al., 2006). A paleoenvironmental model of the whole Kem Kem area is available in Ibrahim et al. (2020).

MINERALOGY

Remarkably, many fossils exhibit soft tissues (muscles, cuticles and gills - Figs. 1C–E - Dutheil, 1999; Garassino et al., 2006; Gueriau et al., 2015) pseudomorphically replaced by nanometric apatite crystallites (< 30 nm), identified as francolite by infrared spectroscopy (Fig. 1F). XRD analyses on oriented preparations indicate that illite and quartz are the main constituents of the bulk sedimentary matrix, with some interstratified illite-smectite minerals and

kaolinite. These minerals are mainly detritic, except for the accordion-like automorphic crystals of kaolinite. Low trace metal concentrations (Fig. DR1C) with very low degree of enrichment (PAAS-normalized enrichment factors for V, Ni, Cu, Zn $\leqslant$ 1.1, Cr ~1.9) and chemical index of alteration of ~78 (Nesbitt and Young, 1982; low range for illite), indicate very moderate weathering. The gypsum crystals filling mudcracks (Fig. 1B and DR5) and the Fe-rich clay minerals displaying plate-like or sheet-like habits forming roses on the sample surface (Figs. 3I and DR5) are clearly secondary (and rather recent), highlighting that sampling and storage conditions have slightly tampered with the samples.

REMAINS OF BIOFILMS

Just as in a textbook case, fossil biofilms can be observed at the OT1 Lagerstätte. They consist in large (tens of cm^2) reddish cracked films lying a few millimeters above each of the fossiliferous layers (Fig. 2A). The morphological similarities between these films (Figs. 2B–D) and modern microbial mats (Fig. 2E) strengthened their identification as well-preserved fossil colonies of microorganisms. Moreover, the fossil skeleton, cuticles and soft tissues (white-to-yellowish in color) are largely covered by similar reddish (to sometimes bluish) thin (a few tens of µm) films (Figs. 1B, 1C, 3A and DR2A) that are interpreted as remains of biofilms. Reddish patches are also found embedded within the phosphatized soft tissues (Figs. 3E, 3F and DR2C), suggesting that their precipitation was concomitant to phosphatization.

A few hundreds of mg of fossil biofilm materials were extracted and milled into powder for XRD analyses, revealing that these mats are composed of $Fe(III)_2O_3$ (iron oxide) minerals (Fig. 2F). µXRF mapping reveals that the iron-rich reddish films covering and embedded within the fossils of teleost fishes and penaeid shrimps *Cretapenaeus berberus* contain trace metals

(Figs. 3A–C, DR1 and DR2), while μXAS investigations at the Fe K-edge reveals that the redox state of iron in these films is identical to that of iron in the mats (+III; Fig. 2G). The spectrum of this Fe-rich mineral is consistent with ferrihydrite (Fe_2O_3•$0.5H_2O$) (Figs. 3G, 3H and DR3), less consistent with goethite (α-FeO(OH)) or lepidocrocite (γ-FeO(OH)), and rather inconsistent with hematite (α-Fe_2O_3) or illite ($(K,H_3O)(Al,Mg,Fe)_2(Si,Al)_4O_{10}[(OH)_2,(H_2O)]$).

ANTIQUITY OF FE-OXIDES

The observed Fe(III) hydroxides surround skeleton tissues and are found around *and within* the phosphatized soft tissues (Figs. 3E and DR2C), suggesting that they precipitated concomitantly with phosphatization. Although some Fe-rich phases in the matrix have been interpreted as resulting from the oxidation of pyrite (e.g., Gabbot et al., 2004; Osés et al., 2016), this is not the case for the observed Fe(III) hydroxides for which a primary origin is more likely. Instead of a cubic or framboidal habit typical of pyrite weathering products, the observed Fe(III) hydroxides show a honeycomb-like morphology, rather typical of microbial mats (e.g., Frankel and Bazylinski, 2003; Davies et al., 2016). In particular, one can observe spherical imprints (Figs. 3J, 3K and DR5), possibly created by coccoid-shaped bacteria (e.g., Iniesto et al., 2016) or gas bubbles having been produced within the microbial mats (e.g., Davies et al., 2016). The fossil biofilms discussed here have thus not been exposed to significant weathering or recrystallization. In other words, the observed Fe(III) hydroxides are likely primary, i.e. they precipitated during the life of the microbial mats, thereby indicating slightly oxic conditions during early diagenesis.

REDOX CONDITIONS DURING PHOSPHATIZATION

Synchrotron-based µXRF analyses of the phosphatic fossil tissues reveal that they incorporated REEs as well as strontium, yttrium and thorium (Fig. 3C). The incorporation of REEs, which substitute for calcium in apatite minerals, generally occurs during diagenesis, with concentrations increasing by three to four orders of magnitude within 10^3-10^4 years depending on diagenetic conditions (Herwartz et al., 2013). The obtained REE patterns display a very limited enrichment in intermediate REEs ("bell-shaped" patterns) and a slightly negative Ce anomaly (Fig. DR4A; Gueriau et al., 2015). The PAAS-normalized La/Yb *vs* La/Sm values confirm that the fossils investigated underwent very limited weathering and recrystallization (Fig. 3D; Reynard et al., 1999; Lécuyer et al., 2003). The observed negative Ce anomaly thus reflects the early diagenetic redox conditions of burial (German and Elderfield, 1990) and points to slightly oxic conditions, consistent with the precipitation of Fe(III) hydroxides. Ce L_3-edge spectroscopy confirms that Ce has a mixed valence (Gueriau et al., 2015), with oxidized Ce (i.e., Ce(IV)) contributing to 20 at.% of the total Ce (Fig. DR4B).

CONCLUSION

Instead of a fall in pH under anoxic conditions, the fine-scale micro-geochemical characterization conducted here strongly suggests that (slightly) oxic conditions prevailed during phosphatization. This conclusion is fully consistent with recent experiment results evidencing that chemical microenvironments generated by microbial mats may turn oxic after several weeks despite initially anoxic conditions (Iniesto et al., 2015). One could argue that the observed Fe(III) hydroxides may have been produced by anaerobic neutrophilic iron oxidizers (e.g., Miot et al., 2009; Hedrich et al., 2011). This would not be inconsistent with the present interpretation, i.e. the establishment of slightly oxic conditions during phosphatization, since neutrophilic iron

oxidizers require the presence of nitrates to survive, i.e., slightly oxic conditions (anaerobic and anoxic are not strict synonyms). Altogether, in contrast to the standard view, the present results establish that exceptional preservation through phosphatization and oxidative conditions are not antithetic.

ACKNOWLEDGMENTS

We acknowledge SOLEIL synchrotron for provision of beamtime under project no. 20131308. J.-G. Bréhéret (Université de Tours) performed and interpreted the XRD analyses on the bulk sediment. V. Beltran and J. Kaddissy (IPANEMA) performed infrared spectroscopy. We thank S. Blanchandin (SOLEIL) for assistance with X-ray powder diffraction of the fossils, D. Vantelon and N. Trcera at the LUCIA beamline (SOLEIL synchrotron), and teams at the Institut des Sciences Analytiques (UMR 5280 CNRS, Lyon, France) and Service d'Analyse des Roches et des Minéraux (CRPG, UMR 7358 CNRS-INSU, Vandœuvre-lès-Nancy) for carrying out the mass spectrometry measurements. The 2012 field expedition and measurements were supported by the MNHN through the "ATM Biodiversité actuelle et fossile" and by the UMR 7207 CR2P. We thank the organizers and field workers of the expedition. This work was developed as part of the IPANEMA / MNHN agreement on collaborative research. IPANEMA is supported by ANR for fast X-ray imaging developments within the PATRIMEX EquipEx (ANR-l1-EQPX-0034). IPANEMA is supported by Région Île-de-France in the context of the DIM "Matériaux anciens et patrimoniaux". We thank Paul Wilson and anonymous reviewers for constructive suggestions to improve the quality of this manuscript.

REFERENCES CITED

Allison, P.A., 1988, The role of anoxia in the decay and mineralization of proteinaceous macro-fossils: Paleobiology, v. 14, p. 139–154, doi:10.1017/S009483730001188X.

Briggs, D.E.G., 2003, The role of decay and mineralization in the preservation of soft-bodied fossils: Annual Review of Earth and Planetary Sciences, v. 31, p. 275–301, doi:10.1146/annurev.earth.31.100901.144746.

Briggs, D.E.G., and Kear, A.J., 1993, Fossilization of soft tissue in the laboratory: Science, v. 259, p. 1439–1442, doi:10.1126/science.259.5100.1439.

Briggs, D.E.G., and Wilby, P.R., 1996, The role of the calcium carbonate-calcium phosphate switch in the mineralization of soft-bodied fossils: Journal of the Geological Society, London, v. 153, p. 665–668, doi:10.1144/gsjgs.153.5.0665.

Davies, N.S., Liu, A.G., Gibling, M.R., and Miller, R.F., 2016, Resolving MISS conceptions and misconceptions: a geological approach to sedimentary surface textures generated by microbial and abiotic processes: Earth-Science Reviews, v. 154, p. 210–246, doi:10.1016/j.earscirev.2016.01.005.

Dutheil, D.B., 1999, An overview of the freshwater fish fauna from the Kem Kem beds (Late Cretaceous: Cenomanian) of southeastern Morocco, *in* Arratia, G., and Schultze, H.-P., eds., Mesozoic Fishes-Systematics and the Fossil Record: Munich, Germany, Verlag Dr. Friedrich Pfeil, p. 553–563.

Föllmi, K.B., 1996, The phosphorus cycle, phosphogenesis and marine phosphate-rich deposits: Earth-Science Reviews, v. 40, p. 55–124, doi:10.1016/0012-8252(95)00049-6.

Frankel, R.B., and Bazylinski, D.A., 2003, Biologically induced mineralization by bacteria: Reviews in Mineralogy and Geochemistry, v. 54, p. 95–114, doi:10.2113/0540095.

Gabbot, S.E., Xian-guang, H., Norry, M.J., and Siveter, D.J., 2004, Preservation of Early Cambrian animals of the Chengjiang biota: Geology, v. 32, p. 901–904, doi:10.1130/G20640.1.

Garassino, A., Pasini, G., and Dutheil, D.B., 2006, *Cretapenaeus berberus* n. gen., n. sp. (Crustacea, Decapoda, Penaeida) from the Late Cretaceous (Cenomanian) of southeastern Morocco: Atti della Società Italiana di Scienze naturali e del Museo civico naturale di Milano, v. 147, p. 3–17.

German, C.R., and Elderfield, H., 1990, Application of the Ce anomaly as a paleoredox indicator: the ground rules: Paleoceanography, v. 5, p. 823–833, doi:10.1029/PA005i005p00823.

Gueriau, P., Mocuta, C., Dutheil, D.B., Cohen, S.X., Thiaudière, D., the OT1 consortium, Charbonnier, S., Clément, G., and Bertrand, L., 2014, Trace elemental imaging of rare earth elements discriminates tissues at microscale in flat fossils: PLoS One, v. 9, e86946, doi:10.1371/journal.pone.0086946.

Gueriau, P., Mocuta, C., and Bertrand, L., 2015, Cerium anomaly at microscale in fossils: Analytical Chemistry, v. 87, p. 8827–8836, doi:10.1021/acs.analchem.5b01820.

Gueriau, P., Jauvion, C., and Mocuta, M., 2018, Show me your yttrium, and I will tell you who you are: implications for fossil imaging: Palaeontology, v. 61, p. 981–990, doi:10.1111/pala.12377.

Hedrich, S., Schlömann, M., and Johnson, D.B., 2011, The iron-oxidizing proteobaxcteria: Microbiology, v. 157, p. 1551-1564, doi:10.1099/mic.0.045344-0.

Herwartz, D., Tütken, T., Jochum, K. P., and Sander, P. M., 2013, Rare earth element systematics of fossil bone revealed by LA-ICPMS analysis: Geochimica et Cosmochimica Acta, v. 103, p. 161–183, doi:10.1016/j.gca.2012.10.038.

Ibrahim, N., Sereno, P.C., Varrichio, D.J., Martill, D.M., Dutheil, D.B., Unwin, D.M., Baidder, L., Larsson, H.C.E., Zouhri, S., Kaoukaya, A., 2020, Geology and paleontology of the Upper Cretaceous Kem Kem Group of eastern Morocco: ZooKeys, v. 928, p. 1–216, doi:10.3897/zookeys.928.47517.

Iniesto, M., Laguna, C., Florín, M., Guerrero, M.C., Chicote, A., Buscalioni, A.D., and López-Archilla, A.I., 2015, The impact of microbial mats and their microenvironmental conditions in early decay of fish: Palaios, v. 30, p. 792–801, doi:10.2110/palo.2014.086.

Iniesto, M., Buscalioni, Á.D., Guerrero, M.C., Benzerara, K., Moreira, D., and López-Archilla, A.I., 2016, Involvement of microbial mats in early fossilization by decay delay and formation of impressions and replicas of vertebrates and invertebrates: Scientific reports, v. 6, 25716, doi:10.1038/srep25716.

Lécuyer, C., Bogey, C., Garcia, J.P., Grandjean, P., Barrat, J.A., Floquet, M., Bardet, N., and Pereda-Superbiola, X., 2003, Stable isotope composition and rare earth element content of vertebrate remains from the Late Cretaceous of northern Spain (Laño): did the environmental record survive? Palaeogeography, Palaeoclimatology, Palaeoecology, v. 193, p. 457–471, doi:10.1016/S0031-0182(03)00261-X.

Martill, D.M., 1988, Preservation of fish in the Cretaceous Santana formation of Brazil: Palaeontology, v. 31, p. 1–18.

Martill, D.M., 1990, Macromolecular resolution of fossilized muscle tissue from an elopomorph fish: Nature, v. 346, p. 171–172, doi:10.1038/346171a0.

Martill, D.M., Ibrahim, N., Brito, P.M., Baider, L., Zhouri, S., Loveridge, R,, Naish, D., and Hing, R., 2011, A new Plattenkalk Konservat Lagerstätte in the Upper Cretaceous of Gara Sbaa, south-eastern Morocco: Cretaceous Research, v. 32, p. 433–446, doi:10.1016/j.cretres.2011.01.005.

McLennan, S.M., 1989, Rare earth elements in sedimentary rocks; influence of provenance and sedimentary processes: Reviews in Mineralogy and Geochemistry, v. 21, p. 169–200.

Meunier-Christmann, C., Lucas, J., and Albrecht, P., 1989, Organic geochemistry of Moroccan phosphorites and bituminous shales. A contribution to the problem of phosphogenesis: Sciences Géologiques, bulletins et mémoires, v. 42, p. 205–222, doi:10.3406/sgeol.1989.1823.

Miot, J., Benzerara, K., Morin, G., Kappler, A., Bernard, S., Obst, M., Férard, C., Skouri-Panet, F., Guigner, J.-M., Posth, N., Galvez, M., Brown Jr., G.E., and Guyot, F., 2009, Iron biomineralization by anaerobic neutrophilic iron-oxidizing bacteria: Geochimica et Cosmochimica Acta, v. 73, p. 696-711, doi:10.1016/j.gca.2008.10.033.

Munoz, M., Argoul, P., and Farges, F., 2003, Continuous Cauchy wavelet transform analyses of EXAFS spectra: A qualitative approach: American mineralogist, v. 88, p. 694–700, doi:10.2138/am-2003-0423.

Nesbitt, H., and Young, G.M., 1982, Early Proterozoic climates and plate motions inferred from major element chemistry of lutites: Nature, v. 299, p. 715–717, doi:10.1038/299715a0.

Osés, G.L., Petri, S., Becker-Kerber, B., Romero, G.R., Rizzutto, M.A., Rodrigues, F., Galante, D., da Silva, T.F., Curado, J.F., Rangel, E.C., Ribeiro, R.P., and Pacheco, M.L.A.F., 2016, Deciphering the preservation of fossil insects: a case study from the Crato Member, Early Cretaceous of Brazil: PeerJ, v. 4, e2756, doi:10.7717/peerj.2756.

Reynard, B., Lécuyer, C., and Grandjean, P., 1999, Crystal-chemical controls on rare-earth element concen- trations in fossil biogenic apatites and implications for paleoenvironmental reconstructions: Chemical Geology, v. 155, p. 233–241, doi:10.1016/S0009-2541(98)00169-7.

Sagemann, J., Bale, S.J., Briggs, D.E.G., and Parkes, R.J., 1999, Controls on the formation of authigenic minerals in association with decaying organic matter: an experimental approach: Geochimica et Cosmochimica Acta, v. 63, p. 1083–1095, doi:10.1016/S0016-7037(99)00087-3.

Wilby, P.R., Briggs, D.E.G., Bernier, P., and Gaillard, C., 1996. Role of microbial mats in the fossilization of soft tissues: Geology, v. 24, p. 787–790, doi:10.1130/0091-7613(1996)024<0787:ROMMIT>2.3.CO;2.

Williams, L.A., and Reimers, C., 1983, Role of bacterial mats in oxygen-deficient marine basins and coastal upwelling regimes: Preliminary report: Geology, v. 11, p. 267–269, doi:10.1130/0091-7613(1983)11<267:ROBMIO>2.0.CO;2.

Wilson, P., Parry, L.A., Vinther, J., and Edgecombe, G.D., 2016, Unveiling biases in soft-tissue phosphatization: extensive preservation of musculature in the Cretaceous (Cenomanian) polychaete *Rollinschaeta myoplena* (Annelida: Amphinomidae): Palaeontology, v. 59, p. 463–479, doi:10.1111/pala.12237.

FIGURE CAPTIONS

Figure 1. The Jebel oum Tkout Lagerstätte (Cenomanian, Morocco). A: Location and map of the Kem Kem area, southeastern Morocco; gray areas denotes the outcrops of the Kem Kem beds. Note the presence of another, slightly younger and marine Lagerstätte at Gara Sbaa (Martill et al., 2011), ca. 15 km southwest of OT1. B: Optical photograph of a gray illitic layer exhibiting mudcracks and topped by a reddish microbial mat. In the center, a paraclupeid fish is visible. C, D: Optical photograph of another paraclupeid (Poi-SGM 10) and SEM images (SE mode) of its finely phosphatized muscles (after Dutheil, 1999: figs. 5 & 6). E: SEM images (SE mode) of mineralized muscles from the penaeid shrimp *Cretapenaeus berberus* (MNHN.F.A24633) (after Garassino et al., 2006: fig. 5). F: Infrared spectrum of mineralized muscles from *C. berberus*. Scale bars: B = 5 cm; C = 5 mm; D = 10 µm; E = 50 µm.

Figure 2. The fossil microbial mats from the Jebel oum Tkout Lagerstätte (Cenomanian, Morocco). A: Optical photograph of an OT1 microbial mat. B–D: SEM images (SE mode) of OT1 microbial mats. E: SEM image (SE mode) of a modern microbial mat for comparison. F: X-ray powder diffraction diagrams of the fossil mat (mat) and of the clayey sedimentary matrix (clay); abbreviations: Qz, quartz; I, illite. Scale bars: A = 1 cm; B–E = 10 µm.

Figure 3. Synchrotron-based µXRF mapping and Fe K-edge µXAS spectroscopy. A: Optical photographs of the teleost fish MHNM-KK-OT 10. B: False color overlays of neodymium (red), yttrium (green) and iron (blue) distributions from the dotted white box area in A. C: Average XRF spectrum and main elemental contributions from the fish dorsal fin muscles (white box in

B). D: PAAS-normalized La/Yb ratios versus La/Sm ratios in OT1 fossils from XRF and ICPMS quantifications reported in the diagrams proposed by Reynard et al. (1999) and Lécuyer et al. (2003). E: Optical photograph of a loose sample containing soft tissues and bone from MHNM-KK-OT 10 (origin: white star in B). F: SEM image (BSE mode) of muscle fibers preserved on the sample in E. G: Normalized μXAS spectra at the Fe K-edge of reference materials (illite, hematite, goethite, lepidocrocite and ferrihydrite) and of iron-rich grains covering the teleost fish (origin: blue star in E) and the penaeid shrimp *Cretapenaeus berberus* (MHNM-KK-OT 01, see Fig. DR2). Spectra were vertically shifted for increased readability. H: Fourier transform magnitude and k^3-weighted μXAS spectra from the iron-rich grains covering the teleost fish (blue) and the shrimp (orange, as well as ferrihydrite (dotted black) and goethite (dotted gray) reference materials. I–K: SEM images (SE mode) of iron oxides (origin: arrows in E). Scale bars: A–B = 5 mm; E = 500 μm; F = 10 μm; I–K = 1 μm.

[1]GSA Data Repository item 202Xxxx, methods, additional synchrotron X-ray fluorescence maps, spectra and main elemental contributions, REEs patterns, Ce L_3-edge spectra, Fe K-edge CCWT modulus, SEM images, precise locations of the point analyses, is available online at www.geosociety.org/pubs/ft20XX.htm, or on request from editing@geosociety.org or Documents Secretary, GSA, P.O. Box 9140, Boulder, CO 80301, USA.

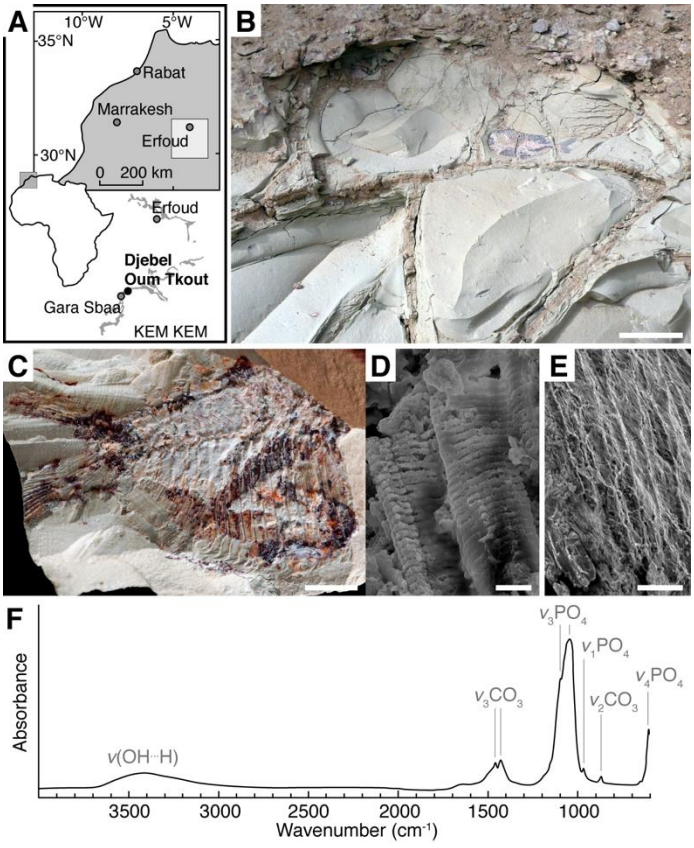

331

332 Figure 1.

333

334

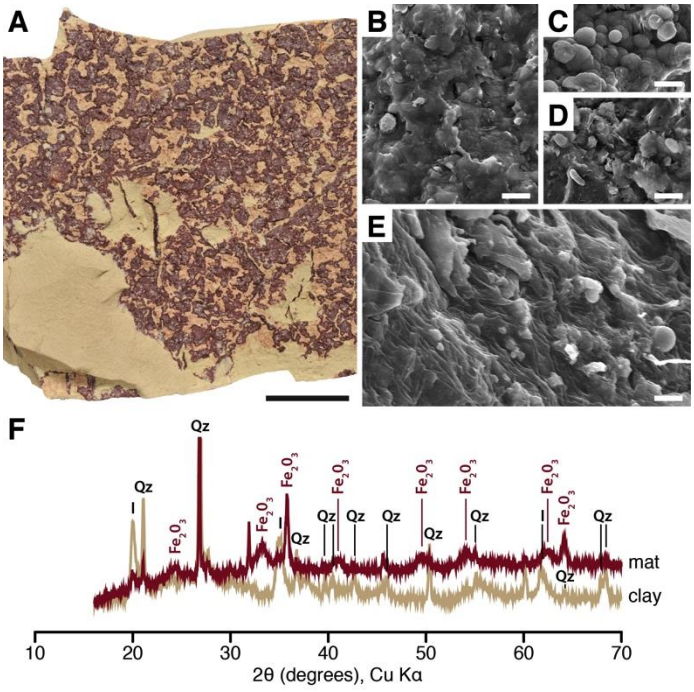

Figure 2.

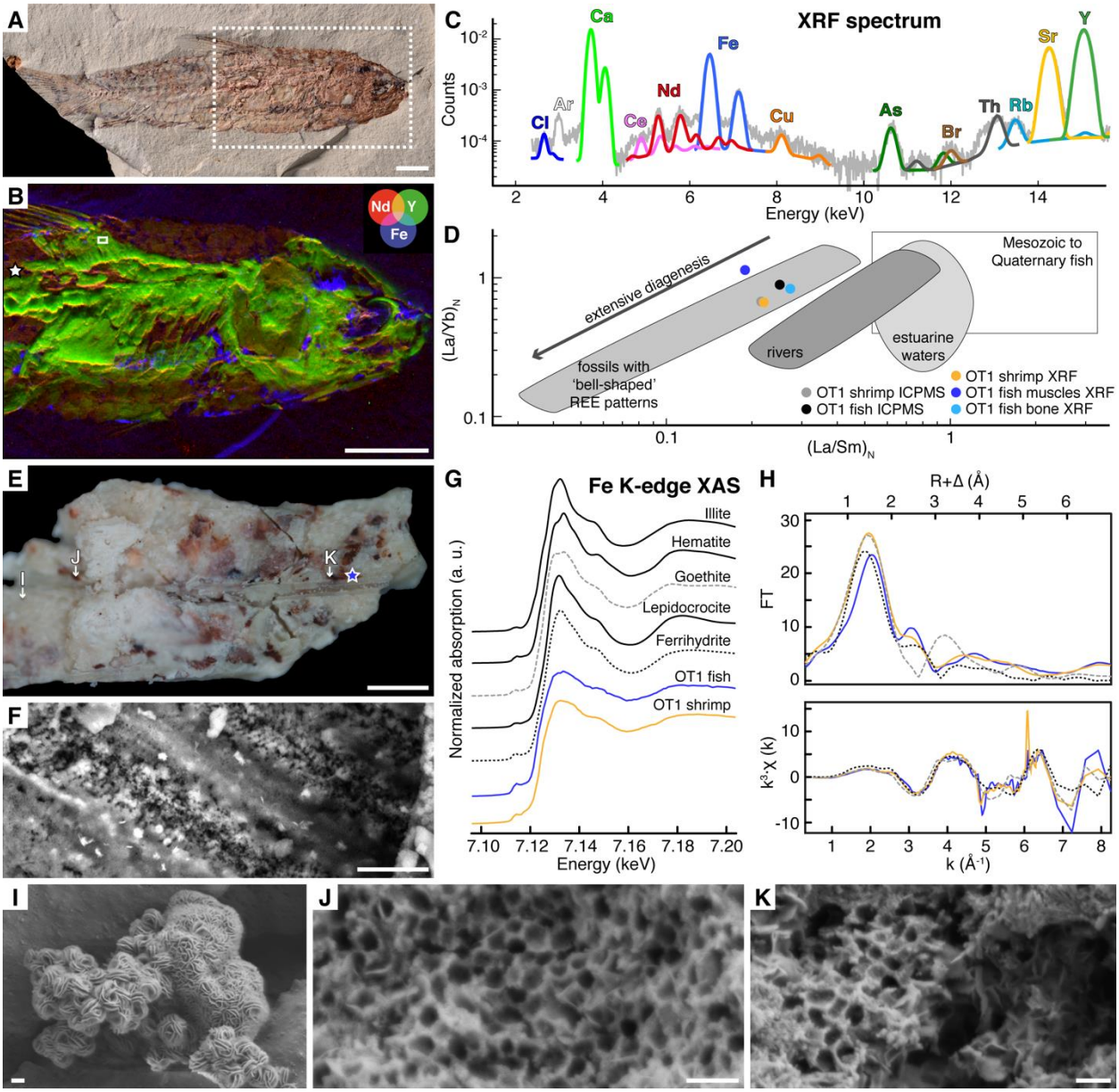

338

339 Figure 3.